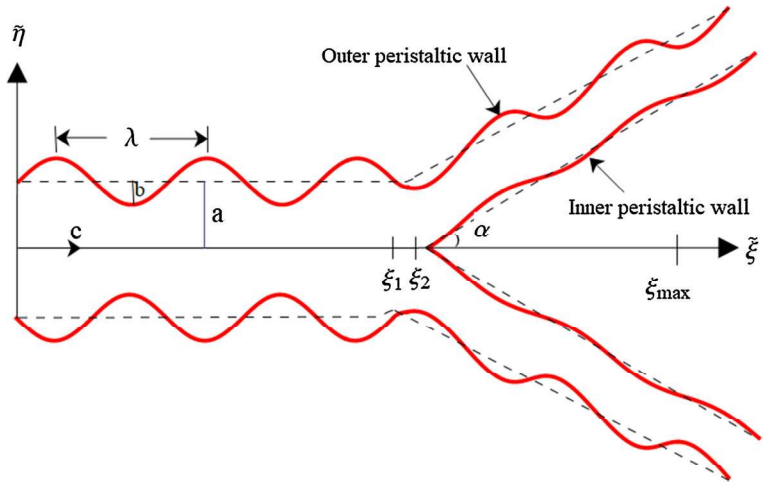

Fig. 1 Geometry of the peristaltic bifurcated channel

The radius of the lateral junction curvatures is $r_0 = \frac{1-2r_1\sec\alpha}{\cos\alpha} - 1$, and the radius of the flow divider curvatures is $\acute{r}_0 = \frac{(x_3-x_2)\sin\alpha}{1-\sin\alpha}$ where x_2, x_3, and x_4 lie on the x-axis of the artery as shown in Fig. 1, which depends on the half of the bifurcation angle α and are written as

$$x_2 = x + x_0 \sin\alpha, \tag{3}$$

$$x_3 = \mathrm{q}_1 + x_2 \text{ and } x_4 = (x - x_3)\tan\alpha - \acute{r}_0(1 - \sin\alpha)\tan\alpha, \tag{4}$$

where $\mathrm{q}_1 \in [0.1, 0.5]$. These values of q_1 show compatibility of the geometry of the bifurcated artery where $H_1(\tilde{x}, \tilde{t})$, $H_2(\tilde{x}, \tilde{t})$ are the expressions for the outward and inward propagating walls of the channel, $\tilde{x}$ is the axial direction coordinate, t represents time, a is the half width of the bifurcated channel, b denotes the amplitude of the walls, λ is the wavelength, and c is the wave velocity, respectively. By considering the bifurcated channel flow to which the inner and outer walls exhibit the sinusoidal wave formation, the values of temperature (T) and nanoparticles' volume fraction (F) at the symmetry line ($\tilde{y} = 0$) are taken as T_0, F_0 and at the bifurcated channel wall ($\tilde{y} = h$) as T_1, F_1, respectively. The nanoparticles' concentration is thin and chooses an appropriate reference pressure.

The governing equations for mass conservation, momentum, thermal energy, and nanoparticles' volume fraction are:

$$\frac{\partial\tilde{u}}{\partial\tilde{x}} + \frac{\partial\tilde{v}}{\partial\tilde{y}} = 0, \tag{5}$$

$$\rho_f\left(\frac{\partial\tilde{u}}{\partial\tilde{t}} + \tilde{u}\frac{\partial\tilde{u}}{\partial\tilde{x}} + \tilde{v}\frac{\partial\tilde{u}}{\partial\tilde{y}}\right) = -\frac{\partial\tilde{p}}{\partial\tilde{x}} + \mu\left(\frac{\partial^2\tilde{u}}{\partial\tilde{x}^2} + \frac{\partial^2\tilde{u}}{\partial\tilde{y}^2}\right)$$
$$+g\left((1 - F_0)\rho_{f0}\beta(T - T_0) - (\rho_p - \rho_{f0})(F - F_0)\right) - \sigma^* B_0^2\tilde{u}, \tag{6}$$

$$\rho_f\left(\frac{\partial\tilde{v}}{\partial\tilde{t}} + \tilde{u}\frac{\partial\tilde{v}}{\partial\tilde{x}} + \tilde{v}\frac{\partial\tilde{v}}{\partial\tilde{y}}\right) = -\frac{\partial\tilde{p}}{\partial\tilde{y}} + \mu\left(\frac{\partial^2\tilde{v}}{\partial\tilde{x}^2} + \frac{\partial^2\tilde{v}}{\partial\tilde{y}^2}\right)$$
$$+g\left((1 - F_0)\rho_{f0}\beta(T - T_0) - (\rho_p - \rho_{f0})(F - F_0)\right), \tag{7}$$

$$(\rho c)_f\left(\frac{\partial T}{\partial\tilde{t}} + \tilde{u}\frac{\partial T}{\partial\tilde{x}} + \tilde{v}\frac{\partial T}{\partial\tilde{y}}\right) = (\rho c)_p\left(D_{\mathrm{B}}\left(\frac{\partial F}{\partial\tilde{x}}\frac{\partial T}{\partial\tilde{x}} + \frac{\partial F}{\partial\tilde{y}}\frac{\partial T}{\partial\tilde{y}}\right) + \frac{D_{\mathrm{T}}}{T_0}\left(\left(\frac{\partial T}{\partial\tilde{x}}\right)^2 + \left(\frac{\partial T}{\partial\tilde{y}}\right)^2\right)\right)$$
$$+\mathrm{k}\left(\frac{\partial^2 T}{\partial\tilde{x}^2} + \frac{\partial^2 T}{\partial\tilde{y}^2}\right), \tag{8}$$

$$(\rho c)_f\left(\frac{\partial F}{\partial\tilde{t}} + \tilde{u}\frac{\partial F}{\partial\tilde{x}} + \tilde{v}\frac{\partial F}{\partial\tilde{y}}\right) = D_B\left(\frac{\partial^2 F}{\partial\tilde{x}^2} + \frac{\partial^2 F}{\partial\tilde{y}^2}\right) + \frac{D_{\mathrm{T}}}{T_0}\left(\frac{\partial^2 T}{\partial\tilde{x}^2}\frac{\partial^2 T}{\partial\tilde{y}^2}\right) \tag{9}$$

where $\tilde{y}$, $\tilde{u}$, $\tilde{v}$, μ, $\tilde{p}$, g, ρ_f, ρ_p, ρ_{f0}, β, $(\rho c)_f$, $(\rho c)_p$, K, T, F, D_{B}, and D_{T} denote transverse coordinate, axial velocity, transverse velocity, pressure, acceleration because of gravity, fluid density, nanoparticles' mass density, nanofluid density at reference temperature (T_0), volumetric expansion coefficient of fluid, heat capacity of fluid, effective heat capacity of nanoparticles, thermal conductivity, temperature, nanoparticle volume fraction, Brownian diffusion coefficient, and thermophoresis diffusion coefficient.

We introduce the non-dimensional parameters:

$$
\begin{aligned}
&x = \frac{\tilde{x}}{\lambda}, y = \frac{\tilde{y}}{a}, t = \frac{c\tilde{t}}{\lambda}, u = \frac{\tilde{u}}{c}, v = \frac{\tilde{v}}{c\delta}, p = \frac{\tilde{p}a^2}{\mu c\lambda}, \delta = \frac{a}{\lambda}, \epsilon = \frac{b}{a}, \theta = \frac{T - T_0}{T_1 - T_0},\\
&\mathrm{M} = B_0\sqrt{\frac{\sigma^*}{\mu}}, \phi = \frac{F - F_0}{F_1 - F_0}, R_e = \frac{\rho_f ca}{\mu}, P_r = \frac{(\rho c)_f\,\mu}{k\rho_{f0}}, G_{r_{\mathrm{T}}} = \frac{\beta\rho_{f0}{}^2a^3\,(1 - F_0)\,(T - T_0)}{\mu^2},\\
&G_{r_F} = \frac{\beta\rho_{f0}a^3\left(\rho_p - \rho_{f0}\right)(F - F_0)}{\mu^2}, N_{\mathrm{b}} = \frac{(\rho c)_p\,D_{\mathrm{b}}\,(F - F_0)}{k}, N_{\mathrm{t}} = \frac{(\rho c)_p\,D_{\mathrm{b}}(T_1 - T_0)}{kT_0},\\
&h_1 = \frac{\tilde{h}_1}{a} = \begin{cases} 1 + \epsilon\sin(2\pi x), & 0 \le x \le x_2 \\ 1 + \epsilon\sin(2\pi x) + r_0 - \sqrt{\left(r_0^2 - (x - x_1)^2\right)}, & x_2 \le x \le x_3 \\ 2r_1 sec\alpha\,(1 + \epsilon\sin(2\pi x)) + (x - x_2)\tan\alpha, & x_3 \le x \le x_{\max} \end{cases},\\
&h_2 = \frac{\tilde{h}_2}{a} = \begin{cases} 0, & 0 \le x \le x_3 \\ \sqrt{\acute{r}_0^2 - \left(x - x_3 - \acute{r}_0\right)^2}, & x_3 \le x \le x_3 + \acute{r}_0(1 - \sin\alpha) \\ \acute{r}_0 cos\alpha\,(1 + \epsilon\sin(2\pi x)) & \\ + \left(x - x_3 - \acute{r}_0\sin\alpha\right)\tan\alpha, & x_3 + \acute{r}_0\,(1 - \sin\alpha) \le x \le x_{\max} \end{cases}
\end{aligned}
\tag{10}
$$

where x is the dimensionless coordinate in the axial direction, y is the dimensionless coordinate in the transverse direction, p is dimensionless pressure, u and v are dimensionless components of velocity, t is dimensionless time, h_1 and h_2 are transverse oscillations of the inner and outer walls, δ is the wave the number, ϵ is the amplitude ratio, v is the kinematic viscosity of the nanofluid, θ is dimensionless temperature, ϕ is nanoparticles' dimensionless volume fraction, $G_{r_{\mathrm{T}}}$ is the thermal Grashof number, G_{r_F} is the basic-density Grashof number, R_e is the Reynolds number, P_r is Prandtl number, N_{t} is the thermophoresis parameter, N_{b} is the Brownian movement parameter, and k the is thermal conductivity of the nanofluid.

Under the approximation of long wavelength (i.e., $k >> a$), we have $\delta \to 0$ and in addition the Reynolds number $R_e \to 0$. While for $\delta \to 0$ the wave effects vanishes, $R_e \to 0$ restrains the convective inertial forces to be negligibly small in relation to the viscous forces. In consideration of these approximations. Eqs. (5)– (9) take the form:

$$\frac{\partial u}{\partial x} + \frac{\partial v}{\partial y} = 0, \tag{11}$$

$$\frac{\partial p}{\partial x} = \frac{\partial^2 u}{\partial y^2} + \sigma^* B_0^2(u + 1) + G_{r_{\mathrm{T}}}\theta - G_{r_F}\Phi, \tag{12}$$

$$\frac{\partial p}{\partial y} = 0, \tag{13}$$

$$\frac{\partial^2\theta}{\partial y^2} + N_{\mathrm{b}}\frac{\partial\theta}{\partial y}\frac{\partial\Phi}{\partial y} + N_{\mathrm{t}}\left(\frac{\partial\theta}{\partial y}\right)^2 = 0, \tag{14}$$

$$\frac{\partial^2\Phi}{\partial y^2} + \frac{N_{\mathrm{t}}}{N_{\mathrm{b}}}\frac{\partial^2\theta}{\partial y^2} = 0. \tag{15}$$

The admissible boundary conditions will be:

$$
\begin{aligned}
&\frac{\partial u}{\partial y} = 0, \theta = 0, \Phi = 0 \text{ at } y = 0, \text{ for } 0 \le x \le x_3,\\
&u = 0, \theta = 0, \Phi = 0 \text{ at } \ y = R_1(x), \text{ for all } x,\\
&u = 0, \theta = 0, \Phi = 0 \text{ at } \ y = R_2(x), \text{ for } x_3 \le x \le x_{\max}.
\end{aligned}
\tag{16}
$$

The effects of bifurcation of the artery can be transmitted into the momentum equations (11) to (15) by reworking on the axial and radial coordinate transformations [1]:

$$\xi = x, \eta = \frac{y - R_2}{R} \tag{17}$$

where $R = R_1 - R_2$.

Using Eq. (17), it is observed that

$$\frac{\partial p}{\partial \xi} = \frac{1}{R^2}\frac{\partial^2 u}{\partial \eta^2} + M^2(u+1) + G_{r_T}\theta - G_{r_F}\Phi, \tag{18}$$

$$\frac{\partial p}{\partial \xi} = 0, \tag{19}$$

$$\frac{1}{R^2}\left(\frac{\partial^2 \theta}{\partial \eta^2} + N_b\frac{\partial \theta}{\partial \eta}\frac{\partial \Phi}{\partial \eta} + N_t\left(\frac{\partial \theta}{\partial \eta}\right)^2\right) = 0, \tag{20}$$

$$\frac{1}{R^2}\left(\frac{\partial^2 \Phi}{\partial \eta^2} + \frac{N_t}{N_b}\frac{\partial^2 \theta}{\partial \eta^2}\right) = 0, \tag{21}$$

and the boundary conditions (16) are

$$\begin{aligned}
&\frac{\partial u}{\partial \eta} = 0, \theta = 0, \Phi = 0 \text{ at } \eta = 0, \text{ for } 0 \le \xi \le \xi_3,\\
&u = 0, \theta = 0, \Phi = 0 \text{ at } \eta = h_1(\xi) \text{ for all } \xi\\
&u = 0, \theta = 0, \Phi = 0 \text{ at } \eta = h_2(\xi) \text{ for } \xi_3 \le \xi \le \xi_{\max}.
\end{aligned} \tag{22}$$

3 Solutions development

We use Cauchy Euler's method to solve the nonhomogeneous ordinary linear differential equation of dependent variables in Eq. (18) which yield velocity profiles for both parent and daughter artery:

$$u(\xi,\eta) = \begin{cases}
\dfrac{\frac{\cosh(M\xi R)}{\cosh(MR)} - 1}{M^2}\dfrac{dP}{dz} - \dfrac{e^{\frac{n}{2}}\left(G_{r_T} + \frac{N_t}{N_b}G_{r_F}\right)\left(\frac{\cosh(M\xi R)}{\cosh(MR)} - 1\right)}{2M^2\sinh\left(\frac{n}{2}\right)}\\
-\dfrac{nG_{r_F}\left(M\xi R - \frac{MR\cosh(M\xi R)}{\cosh(MR)} - \frac{e^{-M\xi R}\left(e^{2M\xi R} - e^{2MR}\right)}{2e^{-MR}\cosh(MR)}\right)}{M^3 R N_b}\\
+\dfrac{R\left(MR\left(\frac{\cosh(M\xi R)}{\cosh(MR)} - e^{n-n\xi}\right) + \frac{n\left(e^{2MR} - e^{2M\xi R}\right)e^{-M\xi R}}{2e^{-MR+n}\cosh(MR)}\right)}{2e^{\frac{n}{2}}M\sinh\left(\frac{n}{2}\right)\left(n^2 - M^2R^2\right)\left(G_{r_T} + \frac{N_t}{N_b}G_{r_F}\right)^{-1}}
\end{cases} \text{ for } 0 \le \xi \le \xi_3$$

$$\text{for } \xi_3 \le \xi \le \xi_{\max} \begin{cases}
\dfrac{4\sinh\left(\frac{MR}{2}\right)\sinh\left(\frac{M(\xi-1)R}{2}\right)\sinh\left(\frac{M\xi R}{2}\right)}{M^2 e^{-MR}(\coth(MR) - 1)^{-1}}\dfrac{dP}{dz}\\
-\dfrac{nG_{r_F}e^{MR}(\sinh(M\xi R) - r\sinh(MR))}{M^2 N_b(\coth(MR) - 1)^{-1}}\\
+\dfrac{\left(\begin{array}{l}
n^2 e^{n - M\xi R}\left(2e^{\frac{3MR}{2}}\sinh\left(\frac{MR}{2}\right) - e^{2M\xi R}\right)\\
M^2R^2 + e^{MR - n\xi}\left(e^{(MR+n)\xi} - 2e^n\sinh(MR)\right)\\
-\left(-e^{MR+n}\begin{pmatrix} M^2R^2e^{-M(\xi-1)R}\\ n^2\cosh(M\xi R)\\ -2\left(n^2 - M^2R^2\right)\sinh(MR)\\ +(n^2 - 2M^2R^2)\sinh(M\xi R)\end{pmatrix}\right)
\end{array}\right)^{\frac{e^{-\frac{n}{2}}}{4M^2}}}{\sinh\left(\frac{n}{2}\right)\left(n^2 - M^2R^2\right)\left(G_{r_T} + \frac{N_t}{N_b}G_{r_F}\right)^{-1}(\coth(MR) - 1)^{-1}}
\end{cases} \tag{23}$$

where the volumetric flow rate of the nanofluid is featured as:

$$\frac{\mathrm{dP}}{\mathrm{d}\xi}=\begin{cases}\dfrac{1}{\begin{pmatrix}(M\sinh(MR)-\cosh(MR)+1)\\ -\mathrm{R}M^2\cosh(MR)\end{pmatrix}}\mathrm{Q}\\ +\dfrac{e^{\frac{n}{2}}\left(G_{r_\mathrm{T}}+G_{r_F}\frac{\mathrm{N_t}}{\mathrm{N_b}}\right)}{2\sinh\left(\frac{n}{2}\right)}\dfrac{\begin{pmatrix}2M\begin{pmatrix}(R+R_2)\sinh(MR)\\ -\cosh(MR)+1\end{pmatrix}\\ -\mathrm{R}\,(\mathrm{R}+2R_2)\cosh(MR)\end{pmatrix}}{\begin{pmatrix}(M\sinh(MR)-\cosh(MR)+1)\\ -\mathrm{R}M^2\cosh(MR)\end{pmatrix}}\\ \mathrm{n}G_{r_F}\mathrm{M}\begin{pmatrix}MR^2\left(\frac{2\mathrm{R}}{3}+R_2\right)-\frac{2MR(M(R+R_2)\sinh(MR))}{M^2\cosh(MR)}\\ -\frac{2\left(-2Me^{MR}(R+R_2)+e^{2MR}(MR_2+1)+MR_2-1\right)}{2M^2e^{-MR}cosh(MR)}\\ +\frac{2MR(M(R+R_2)\sinh(MR)-\cosh(MR)+1)}{M^2\cosh(MR)}\\ -\frac{2R^2}{3}+\frac{2MR(-\cosh(MR)+1)}{M^2\cosh(MR)}+\mathrm{M}R^2R_2\end{pmatrix}\\ +\dfrac{}{2R\mathrm{N_b}\sec h(MR)\begin{pmatrix}(M\sinh(MR)-\cosh(MR)+1)\\ -\mathrm{R}M^2\cosh(MR)\end{pmatrix}}\end{cases}\quad\text{for}\quad 0\le\xi\le\xi_3$$

$$\begin{cases}-\dfrac{(\coth(MR)-1)^{-1}\mathrm{M}e^{-MR}}{\sinh\left(\frac{MR}{2}\right)(R+2R_2)\left(MR\cosh\left(\frac{MR}{2}\right)-2\sinh\left(\frac{MR}{2}\right)\right)}Q\\ +\dfrac{\mathrm{n}G_{r_F}e^{MR}\begin{pmatrix}\frac{M(R+R_2)\cosh(MR)-\sinh(MR)-MR_2}{M^2}\\ -\frac{1}{6}\sinh(MR)R(2R+3R_2)\end{pmatrix}\mathrm{M}e^{-MR}}{\mathrm{N_b}\sinh\left(\frac{MR}{2}\right)(R+2R_2)\left(MR\cosh\left(\frac{MR}{2}\right)-2\sinh\left(\frac{MR}{2}\right)\right)}\\ -\mathrm{M}\dfrac{\begin{pmatrix}n^2e^n\begin{pmatrix}2e^{\frac{3MR}{2}}\sinh\left(\frac{MR}{2}\right)\frac{e^{-MR}\left(-M(R+R_2)+e^{MR}(MR_2+1)-1\right)}{M^2}\\ -\frac{e^{MR}(M(R+R_2)-1)-MR_2+1}{M^2}\end{pmatrix}\\ M^2R^2+e^{MR}\begin{pmatrix}\frac{e^{MR}(M(R+R_2)-1)-MR_2+1}{M^2}\\ -2\frac{e^{-n}R((-n+e^n-1)R+(e^n-1)nR_2)}{n^2e^{-n}\cos\mathrm{ceh}(MR)}\end{pmatrix}\\ -\begin{pmatrix}M^2R^2\frac{e^{-MR}(-M(R+R_2)+e^{MR}(MR_2+1)-1)}{M^2e^{-MR}}\\ -e^{MR+n}\begin{pmatrix}n^2\frac{M(R+R_2)\sinh(MR)-\cosh(MR)+1}{M^2}\\ -2\left(n^2-M^2R^2\right)\sinh(MR)\,R\left(\frac{R}{2}+R_2\right)\\ +\frac{M(R+R_2)\cosh(MR)-\sinh(MR)-MR_2}{M^2(n^2-2M^2R^2)^-}\end{pmatrix}\end{pmatrix}\end{pmatrix}}{4\sinh\left(\frac{MR}{2}\right)\sinh\left(\frac{n}{2}\right)e^{-MR+\frac{n}{2}}\left(n^2-M^2R^2\right)\left(G_{r_\mathrm{T}}+G_{r_F}\frac{\mathrm{N_t}}{\mathrm{N_b}}\right)^{-1}}\\ \times(R+2R_2)\left(MR\cosh\left(\frac{MR}{2}\right)-2\sinh\left(\frac{MR}{2}\right)\right)\end{cases}\quad\text{for}\quad \xi_3\le\xi\le\xi_{\max},\tag{24}$$

$$Q_p = 2R \int_0^1 \tilde{u} \mathrm{d}y, \tag{25}$$

$$Q_d = R \int_0^1 \tilde{u} \mathrm{d}y. \tag{26}$$

The conversion between a wave framework $(\tilde{X}, \tilde{Y})$ progressing with velocity c and the fixed framework $\tilde{x}$, $\tilde{y}$ is presented as [2,3]:

$$\tilde{X} = \tilde{x} - c\tilde{t}, \quad \tilde{Y} = \tilde{y}, \quad \tilde{U} = \tilde{u} - c, \quad \tilde{V} = \tilde{v},$$

where $\left(\tilde{U}, \tilde{V}\right)$ and $(\tilde{u}, \tilde{v})$ are the velocity arguments in the oscillatory and fixed framework, respectively. The volumetric flow rate in the waving frame may be worked out with the following expressions:

$$Q_p = 2R \int_0^1 (U + 1)\, dY, \tag{27}$$

$$Q_d = R \int_0^1 (U + 1)\, dY, \tag{28}$$

and integration leads to:

$$Q_p = 2R\,(q + 1)\,, \tag{29}$$

$$Q_d = R\,(q + 1) \tag{30}$$

where $q = \int_0^1 U dY$.

Volumetric flow rate averaging over one period of time yields:

$$\bar{Q}_p = \int_0^1 Q_p \mathrm{d}t = \int_0^1 2R\,(q + 1)\,\mathrm{d}t, \tag{31}$$

$$\bar{Q}_d = \int_0^1 Q_d \mathrm{d}t = \int_0^1 R\,(q + 1)\,\mathrm{d}t, \tag{32}$$

Using Eqs. (31) and (32), it is observed that:

$$\bar{Q}_p = 2RQ_p, \tag{33}$$

$$\bar{Q}_d = RQ_d. \tag{34}$$

The pressure across one wavelength is

$$\Delta P = \int_0^1 \left(-\frac{\partial P}{\partial \xi}\right) d\xi. \tag{35}$$

The resistance to the blood flow is described as

$$\lambda = \frac{\Delta P}{Q}. \tag{36}$$

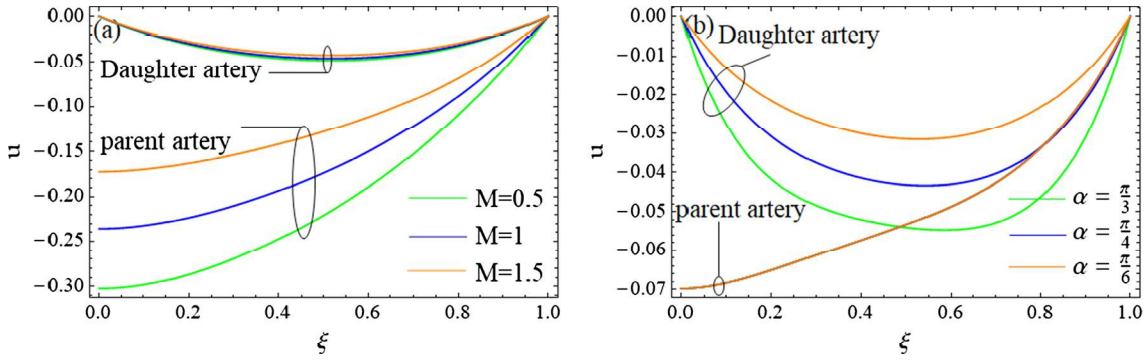

Fig. 2 Velocity profiles (u) for different values of the Hartmann number (M) and bifurcation angle (α) (shown by panels **a** and **b**, respectively)

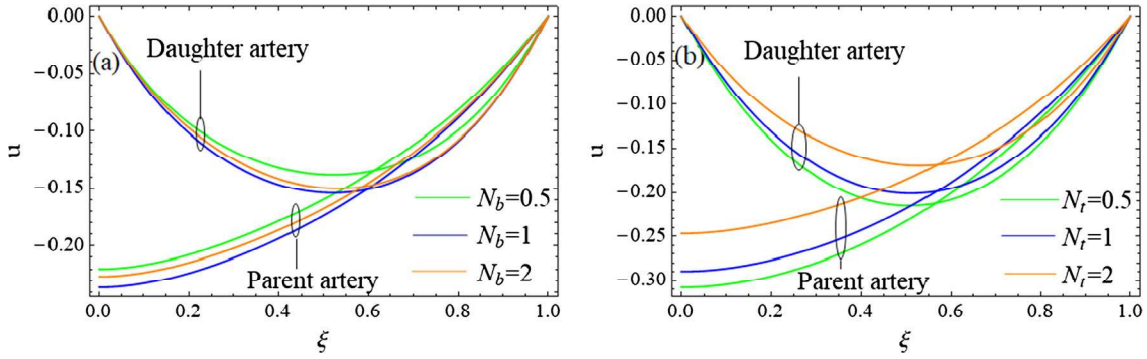

Fig. 3 Velocity profiles (u) for different values of Brownian motion parameter (N_b), thermophoretic parameter (N_t) (shown by panels **a** and **b**, respectively)

4 Graphical results and discussion

This study becomes interested or engaged in order to determine the quantitative effects of magnetohydrodynamics and nanoparticles on peristaltic flow through a bifurcated channel in the present section. An illustration with graphical results is presented in Figs. 2, 3, 4, 5, 6, 7, 8, 9, 10, and 11 to demonstrate the influence of the various physical parameters on the blood flow features by considering that $d = 4, \alpha = \frac{\pi}{6}, ir_1 = 0.45, q = 0.5, \xi_1 = 12, \xi_m = 20, Q = 0.1, \frac{\mathrm{d}P}{\mathrm{d}z} = 1, \epsilon = 0.2$. The results are achieved by using Mathematica notebook.

Figures 2, 3, and 4 give a visible impression of different parameters on the velocity profiles in the bifurcated artery. In these Figures, the axial velocity is generally negative for both parent channel and daughter artery, which means flow reversal or back flow is taking place. The axial velocity is maximum at the center ($\xi = 0$) in the parent artery and parabolically symmetric in the daughter artery that maximizes at $\xi = 0.5$. Figure 2a shows the Hartmann number depending on the velocity of the fluid. It is seen that with the increase in Hartmann number (M) the magnitude of the velocity profile decreases in both parent and daughter arteries, whereas the magnitude of velocity curves begins to increase in the parent artery as compared to the velocity in the daughter artery. The Hartmann number supports the backflow in the bifurcated artery. This is physically described as the magnetic field applications on electrically conducting nanofluid producing a resistive force in order to slow the flow in which viscous forces influence the electrical conductivity. Figure 2b shows the changes occurring in the velocity profile with the change in the bifurcated angles. It is disclosed that with the increase in the bifurcation angle (α) the velocity exhibits no change in the parent artery while its magnitude decreases with the increase in the bifurcation angle.

Figure 3 shows the variation velocity profiles (u) for different values of the Brownian motion parameter (N_b) and thermophoresis parameter (N_t). Figure 3a indicates that with the increase in the Brownian motion parameter (N_t) there has been a decrease in the magnitude of the velocity profile which is observed in both parent and daughter artery. Physically this means that the nanoparticle volume fraction is responsible to make

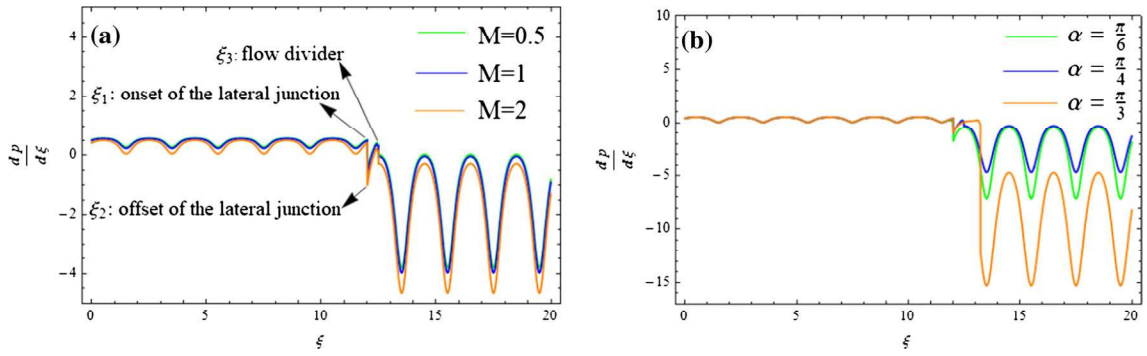

Fig. 8 Pressure gradient $\left(\frac{\mathrm{d}p}{\mathrm{d}\xi}\right)$ versus axial direction (ξ) with variation of magnetic field (M) and bifurcation angle (α) (shown by panels **a** and **b**, respectively)

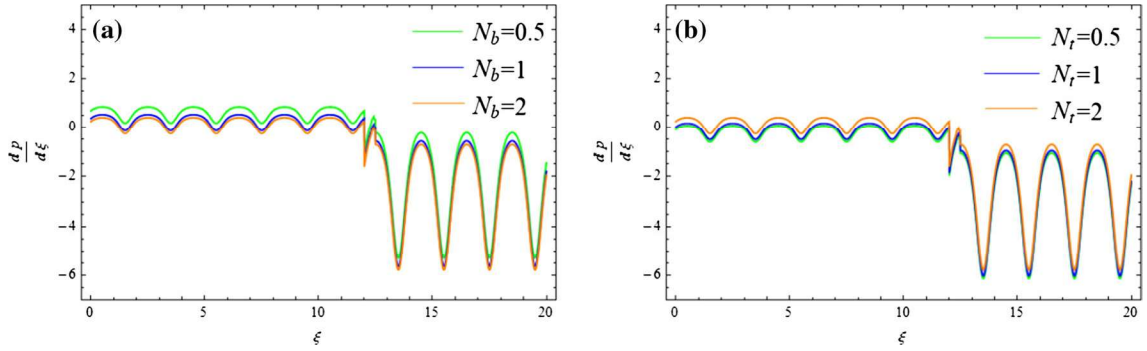

Fig. 9 Pressure gradient $\left(\frac{\mathrm{d}p}{\mathrm{d}\xi}\right)$ vs axial direction (ξ) with variation of Brownian motion parameter (N_b) and thermophoresis parameter(N_t) (shown by panels **a** and **b**, respectively)

by viscous forces and vice versa for $Gr_\mathrm{T} > 1$. For the intermediate instance of $Gr_\mathrm{T} = 1$, both thermal buoyancy and viscous forces are equal with order of magnitude. Pressure differences are generally enhanced with increasing thermal Grashof number. Figure 7b discloses that the influence of the species basic-density Grashof number (Gr_F) on the pressure difference is also enhanced to that of the thermal Grashof number. Increasing (Gr_F) signifies the fraction of species buoyancy forces to the viscous hydrodynamic forces. For the case where both forces are the same, i.e., $Gr_\mathrm{F} = 1$ is situated as intermediate pressure difference. The pressure difference remains above in the region ($-1 \leq Q \leq 0$) for the daughter artery, and the reverse trend is observed in the region ($0 \leq Q \leq 1$) for the parent artery.

Figures 8, 9, and 10 are representing the effects of Hartman number (M), bifurcation angle (α), thermophoresis parameter (N_t), Brownian motion parameter(N_b), thermal Grashof number (G_{r_T}), and species Grashof number (G_{r_F}) on the pressure gradient $\left(\frac{\mathrm{d}p}{\mathrm{d}\xi}\right)$ on both sides of the apex. Clearly, the pressure gradient is of sinusoidal form in parent and daughter artery, and the amplitude in the parent artery is significantly lower than the amplitude in the daughter artery. From Fig. 8a, it is seen that the pressure gradient is decreasing with an increase in the value of the Hartman number (M), and from Fig. 8b it is also seen that the pressure gradient remains the same in the parent artery whereas it decreases in the daughter artery with the increase in the bifurcation angle (α). From Fig. 9a, it is seen that the pressure gradient is decreasing with an increase in the value of Brownian motion parameter (N_b), and from Fig. 9b it is also seen that the pressure gradient increases with the increase in thermophoresis parameter (N_t) in both parent and daughter artery. From Fig. 10a, b, it is seen that the pressure gradient is increasing with an increase in the value of thermal Grashof number (G_{r_T}) and species Grashof number (G_{r_F}) in both parent and daughter artery.

From Figures 8, 9, and 10, it is seen that the pressure gradient behaves in a normal manner, but it flustered moderately near the flow divider in the parent artery due to the degeneration at the start of the flow divider. All the profiles are locally increased until the inset of lateral junction then small decrease is exhibited, and then increases until the flow divider. Thereafter, it starts sinusoidal behavior with attaining longer amplitude because of the diverging of the blood flow at bifurcation of the artery.

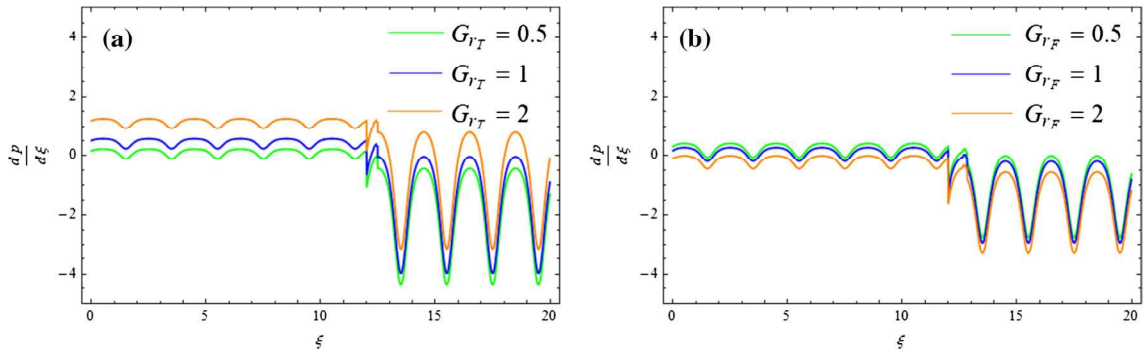

Fig. 10 Pressure gradient $\left(\frac{\mathrm{d}p}{\mathrm{d}\xi}\right)$ vs axial direction (ξ) with different values of thermal Grashof number (G_{r_T}) and species Grashof number (G_{r_F}) (shown by panels **a** and **b**, respectively)

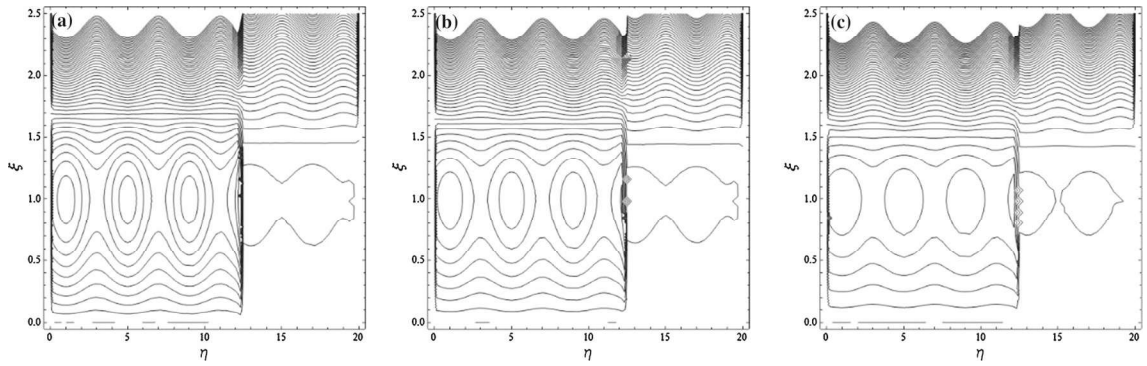

Fig. 11 Plot shows streamlines for different values of the magnetic field M. **a** $M = 0.5$, **b** $M = 1$, **c** $M = 2$

Table 1 Resistance (turbulence) λ for different amplitudes of the walls for all values of axial distance ξ

λ		$M = 0.5$	$M = 1$	$M = 2$
$\epsilon = 0$	Parent artery	3.2407	3.01278	2.1146
	Daughter artery	− 8.0721	− 8.9740	− 12.5659
$\epsilon = 0.1$	Parent artery	3.4081	3.2050	2.4072
	Daughter artery	− 5.4942	− 6.2940	− 9.4777
$\epsilon = 0.2$	Parent artery	3.5265	3.3435	2.6261
	Daughter artery	− 3.6791	− 4.3967	− 7.2513

The streamlines on the central line in the frame are structured under specific conditions in order to encircle a bolus of fluid particles circulating together with closed streamlines. This occurrence is recognized as trapping, which is the peristaltic motion, as given in detail by Fung and Yih [30], and trapping for stenotic arteries is discussed by Ahmed and Nadeem [31–34]. Figure 11 shows that the trapping bolus size is enhanced by escalating the magnetic field in the parent artery section while the boluses are grown in the daughter artery by enhancing the magnetic field.

The turbulence increases the resistance dramatically so that large increases in pressure will be required to further increase the volume flowrate. From Table 1, it is noticed that with the increase in the magnetic field the resistance decreases, so the phenomena control the turbulence in the flow field in the bifurcated artery for all values along the axial distance ξ. At low Reynolds numbers, the flows tend to be dominated laminar (sheet-like) as performed in this study, while at high Reynolds numbers turbulence results.

5 Concluding remarks

The examination of nanofluid is featuring heat transfer within the axisymmetric two-dimensional bifurcated peristaltic channel. It were developed closed-form analytical solutions with the **Mathematica** applications. The